Inhomogeneity effects in a gas laser

Guy Stephan and Manfred Trümper*
Equipe (No. 748) de Recherche associée au Centre National de la Recherche Scientifique, Laboratoire de Spectroscopie, Université de Rennes, avenue du Général Leclerc, F-35042 Rennes, France
(Received 20 October 1982)

We show that in a gas laser the inhomogeneity in the distribution of amplifying atoms and the transverse Gaussian distribution of the saturating electromagnetic field give rise to different lens effects which are generally opposite to each other and influence the line shapes in different ways, shifting the Lamb dip either to the blue or to the red. For those laser phenomena which increase one or the other of the lens effects, the role of a diaphragm is of particular importance, since it determines the spatial distribution of the resonant field. We present here a new method for studying the resonant diffracted field in a laser. Also, we give a unified description of the various inhomogeneities. Doing away with the usual method of mean-field approximation, we numerically calculate, for a diaphragmed, monomode weak-gain gas laser, the intensity, variation of the beam diameter, and the radius of curvature as functions of the frequency.

INTRODUCTION

During the past two decades, laser theory has been dominated by the so-called "mean-field approximation," first introduced by Lamb.[1] The model is based on a hypothetical medium whose gain (due to the amplifying medium) and losses (due to diffraction and mirrors) are uniformly distributed. The field is supposed to be composed of plane waves, but the field amplitude entering the saturation terms is taken as a (coordinate-independent) constant. This approximation has proved to be quite successful in explaining properties[2] of radiation from gas lasers, such as, for instance, the celebrated Lamb dip. Early theories gave symmetric line shapes, but experiments showed asymmetries[3] which were first attributed to atomic collisions.[4] Then, after Kogelnik[5] studied Gaussian beams, Maeda and Shimoda[6] showed that the corresponding line shapes were strongly asymmetric. However, in this theory, the diameter of the mode was supposed to remain uniform along the laser axis, so that, again, some kind of mean-field approximation has been used, this time along the laser axis. On the experimental side, Garside has shown that the transverse nonuniformity of the field is at the origin of lens effects which result in the change of the beam diameter with frequency, thus giving rise to frequency-dependent losses which, in turn, could explain the observed asymmetry of line shapes.[7] This has been experimentally confirmed in a single-mode HeNe laser.[8] Another transverse effect, the inhomogeneity of amplifying atoms, was used by Casperson and Yariv[9] to explain asymmetries which they observed in a high-gain gas laser.

Asymmetries of line shapes actually originate from various causes[10] which may be subdivided into microscopic (related to atoms) and macroscopic ones. We will be concerned only with the second kind.

A theoretical study of resonant self-focusing and defocusing effects of Gaussian beams in weak-gain gas lasers has been made recently by Stephan and Taleb.[11] It was shown that the two transverse parameters W (beam diameter) and R (radius of curvature) vary with frequency. As a consequence, the measured line shapes vary with the aperture of the detector. This finding has been experimentally confirmed.[12]

The aim of the present work is to leave behind the mean-field approximation and to study a real monomode gas laser equipped with a diaphragm to suppress transverse modes, taking into account localized gain and losses, a nonuniform distribution of amplifying atoms, and a nonuniform field.

The new approach makes possible the study of effects (e.g., influence on line shapes) due to

(i) the self-focusing or defocusing,
(ii) the population inhomogeneity,
(iii) diffraction,
(iv) the geometrical parameters of the cavity.

The results are obtained by first setting up the nonlinear differential equations and then by integrating them numerically under the boundary con-

ditions imposed by the mirrors.

They show that, generally, there is a kind of competition between the lens effects due (a) to saturation, and (b) to the transverse distribution of active atoms. If the effect of (a) is greater (smaller) than the effect of (b), the maximum intensity of the line is on the low- (high-) frequency side. Because of their strong influence on the field, the competition is very sensitive to the laser properties such as the geometry (length, radius of curvature of the mirrors, position of the diaphragm, and diameter of the tube) or the distribution of atoms dependent on the discharge current.

The paper is organized as follows. In Sec. I we review the theory of a Gaussian beam in a nondiaphragmed laser. We start from the passive cavity and, following Lax *et al.*,[13] we obtain the beam equation in the paraxial approximation. Using scaled coordinates we give a simplified treatment of Gauss-Laguerre modes. Then we consider the cavity with an amplifying medium and establish the inhomogeneous beam equation whose solutions are written as modified Gauss-Laguerre modes. Such solutions have already been recognized,[14] but our interpretation is somewhat different. We show that inhomogeneities modify the diameter and radius of curvature of a beam along the laser axis and we obtain equations for these modifications. In Sec. II we consider a diaphragmed laser and we start with an empty diaphragmed cavity in order to calculate the resonant diffracted eigenfield. This field is developed on the basis of the preceding modes and we compute the eigenfield having the highest eigenvalue (i.e., having the lowest diffraction losses) along the laser axis. Equations for the field in the cavity with an amplifying medium are then given and solved numerically. In the case of the 3.39-μm line of Ne, results concerning the dependence of intensity, radius of curvature, and diameter of the beam on the frequency are given for various values of those parameters which are essential in the description of inhomogeneities. The role of other parameters, also important in studies of laser line shapes (e.g., the length of the laser and the length and position of the amplifying tube), will be studied in later work.

I. THEORY OF A GAUSSIAN BEAM IN A NONDIAPHRAGMED LASER

It is well understood that the laser phenomenon owes its existence to those two parts of the experimental setup which are most simply described by notions as "Fabry-Perot interferometer" (the cavity) and "amplifying medium." It is the former one which allows for constructive interference between the forward and the backward beam and it is the latter one which sustains the radiation field by compensating the losses.

Accordingly, the task of describing the geometry of laser beams is subdivided into two parts. First, the treatment of a beam from an external source passing forth and back in a "passive cavity," i.e., one which does not sustain the oscillation. The medium is characterized by a polarizability which is independent of the field. Second, the laser in its proper state of operation, in which the polarizability of the medium depends strongly on the electric field.

A. The passive cavity

1. Helmholtz equation in the paraxial approximation

By the shape and arrangement of the mirrors one assures the low divergence (parallelism of rays) of the laser beam which is necessary for the continuous production of laser light. This property of the beam allows to simplify the theoretical treatment by means of the so-called paraxial approximation.

The usual starting point for the treatment of laser beams are the Maxwell equations for the electromagnetic field $\vec{E}$ inside the cavity:

$$\mathrm{curl}\vec{E}=-\partial\vec{B}/\partial t,\quad \mathrm{curl}\vec{H}=\partial\vec{D}/\partial t\ , \tag{1}$$

$$\mathrm{div}\vec{D}=0,\quad \mathrm{div}\vec{B}=0\ , \tag{2}$$

$$\vec{D}=(\epsilon_0+\alpha)\vec{E},\quad \vec{B}=\mu_0\vec{H}\ . \tag{3}$$

They give rise to the propagation equation

$$-\mathrm{grad}(\mathrm{div}\vec{E})+\Delta\vec{E}=\left[\frac{1}{c^2}+\mu_0\alpha\right]\frac{\partial^2\vec{E}}{\partial t^2}\ , \tag{4}$$

which is to be satisfied by a monochromatic wave traveling along the axis of a laser tube (aligned with the z direction):

$$\vec{E}(\vec{r},t)=\vec{F}(\vec{r})\exp[i(kz-\omega t)]\ . \tag{5}$$

In order to allow for emission and absorption processes (described phenomenologically by a complex polarizability α), the electric field (and hence the quantity $\vec{F}$) is assumed to be a complex vector. The polarizability is written as $\alpha=\alpha_0+\alpha_n$, where α_0 is a complex constant describing the linear homogeneous medium, whereas the variable α_n may express spatial inhomogeneity as well as the saturation. It should be noted that in the type of gas laser studied here we have a ratio of $|\alpha_0/\epsilon_0|\sim 10^{-5}$.

A brief discussion of the meaning of Eq. (5) appears to be indicated. If $\vec{F}(\vec{r})$ were a constant, (5) would simply represent a plane wave. If $\vec{F}$ were a real function of the spatial coordinates, one could visualize the field $\vec{E}$ as follows. Consider any straight line parallel to the laser axis (in particular,

e.g., the axis itself). Along such a line, the transverse coordinates x and y are constant and the field has the form $\vec{F}(z)\exp[i(kz-\omega t)]$. At an instant $t=$const this is a wave with wavelength $2\pi/|k|$ whose amplitude is modulated by the function $\vec{F}(z)$. However, for this interpretation to be valid one has to assume that at any extremum of the wave, the amplitude function $\vec{F}(z)$ is less curved than the wave itself. Otherwise, the wave structure would cease to exist. It is thus clear that factorizing $\exp(ikz)$ in (5) only makes sense if one demands, in addition, that the variation of the remaining field $\vec{F}(z)$ is sufficiently slow in the variable z. Now, as the function $\vec{F}(z)$ in Eq. (5) is a complex one and its phase gives rise to a z-dependent change of the wavelength, we have not only to demand that the absolute value of $\vec{F}$, but also that its phase varies slowly with z.

Of course, these assumptions are consistent with the physical nature of a laser beam whose intensity varies much more in transverse direction than longitudinally, so that transverse and longitudinal derivatives of the field have different magnitudes.

To gain control over the rate of change of $\vec{F}$ with z, Lax *et al.*[13] introduced dimensionless coordinates which were obtained by scaling x and y with W_0, the beam radius at the waist, and z with the factor $|k|W_0^2$. But this parameter W_0 itself resulted from a theoretical treatment the criticism of which motivated the investigation.[13] We feel, therefore, that it is more satisfactory to start by assuming that there is some characteristic length l_0 given by the experimental setup, and to identify this length with a suitable physical quantity only after the quantity has emerged from the calculation. (For a laser configuration which produces a beam having axial symmetry, we may, from the outset, consider l_0 as a characteristic transverse falloff length.)

The dimensionless quantity [we are using the symbol := (or =:) to mean "equal by definition," with the ":" on the side of the quantity which is being defined.]

$$\mu := c/\omega l_0$$

which is assumed to be much smaller than 1, gives rise to two separate length scales, one for the transverse and the other for the longitudinal distance. At the same time, the length l_0 will be used to introduce dimensionless variables. Following (in essence) Lax, Louisell, and McKnight[13] we define new coordinates

$$\xi := x/l_0, \quad \eta := y/l_0, \quad \zeta := \mu z/l_0 \tag{6}$$

and, thereby, the differentiation operators

$$\partial_x = l_0^{-1}\partial_\xi, \quad \partial_y = l_0^{-1}\partial_\eta, \quad \partial_z = \mu l_0^{-1}\partial_\zeta . \tag{7}$$

As the new coordinate ζ will no longer be treated on the same footing as the "transverse" coordinates ξ and η, Eq. (5) as well as the vectors involved will now be decomposed into a transverse part $\vec{F}_T$ and a longitudinal part F_ζ. Note that $\vec{F}_T$ is a vector and $\vec{\nabla}_T$ is the differentiation operator in the $\xi\eta$ plane. The resulting equations, obtained from (4), are

$$-\vec{\nabla}_T(\vec{\nabla}_T\cdot\vec{F}_T+\mu\partial_\zeta F_\zeta+i\mu^{-1}F_\zeta)+(\nabla_T^2+\mu^2\partial_\zeta^2+2i\partial_\zeta-k^2l_0^2)\vec{F}_T=-\frac{\omega^2 l_0^2}{c^2}\left[1+\frac{\alpha}{\epsilon_0}\right]\vec{F}_T , \tag{8}$$

and

$$-\mu\partial_\zeta(\vec{\nabla}_T\cdot\vec{F}_T)-i\mu^{-1}\vec{\nabla}_T\cdot\vec{F}_T+\nabla_T^2F_\zeta=-\frac{\omega^2 l_0^2}{c^2}\left[1+\frac{\alpha}{\epsilon_0}\right]F_\zeta . \tag{9}$$

In deriving these equations we have approximated the complex "wave number"

$$k=\frac{\omega}{c}\left[1+\frac{\alpha_0}{\epsilon_0}\right]^{1/2} \tag{10}$$

by the real quantity ω/c. If the term on the right-hand side of (8) is rewritten as $-k^2l_0^2-l_0^2\omega^2\alpha_n/\epsilon_0c^2$ we notice that the first term in this expression cancels the last term on the left-hand side.

Multiplying (8) with μ and (9) with μ^2 we now get

$$-\vec{\nabla}_T(\mu\vec{\nabla}_T\cdot\vec{F}_T+\mu^2\partial_\zeta F_\zeta+iF_\zeta)+\mu\nabla_T^2\vec{F}_T$$
$$+\mu^3\partial_\zeta^2\vec{F}_T+2i\mu\partial_\zeta\vec{F}_T=-\mu^{-1}\frac{\alpha_n}{\epsilon_0}\vec{F}_T , \tag{11}$$

$$-\mu^3\partial_\zeta(\vec{\nabla}_T\cdot\vec{F}_T)-i\mu\vec{\nabla}_T\cdot\vec{F}_T+\mu^2\nabla_T^2F_\zeta$$
$$=-(1+\alpha/\epsilon_0)F_\zeta . \tag{12}$$

These equations are the starting point for the paraxial approximation: Formal series for the functions $\vec{F}_T$ and F_ζ (with μ as the development parameter) are inserted into (11) and (12), and the coefficients of equal powers in μ are then compared. In this way one gets a sequence of differential equations which can be solved by iteration.

According to Eq. (12), F_ζ is small, of order one, thus it is small compared to $\vec{F}_T$. Therefore, the series can be written as

$$\vec{F}_T=\vec{F}_T^0+\mu\vec{F}_T^1+\mu^2\vec{F}_T^2+\cdots ,$$

$$F_\xi=\mu F_\xi'+\mu^2F_\xi^2+\cdots .$$

In the remainder of Sec. I A we will assume that α/ϵ_0 is of order 3 in μ. (As we are treating here the case of a passive cavity we could as well put $\alpha=0$, but we wish to indicate the degree of generality under which the following results will hold.)

We then get, in lowest order,

$$-\vec{\nabla}_T(\vec{\nabla}_T\cdot\vec{F}_T^0+iF_\xi^1)+\nabla_T^2\vec{F}_T^0+2i\partial_\xi\vec{F}_T^0=0 , \quad (13)$$

$$-i\vec{\nabla}_T\cdot\vec{F}_T^0+F_\xi^1=0 . \quad (14)$$

Equation (13), simplified by (14), now gives

$$\nabla_T^2\vec{F}_T^0+2i\partial_\xi\vec{F}_T^0=0 . \quad (15)$$

This equation may be considered as the fundamental equation of Gaussian beam optics. It will henceforth be referred to as the "beam equation," and any physically acceptable solution of it will be called a "beam function."

In the following we will be concerned with linearly polarized light and the transverse electric field will have one single component. Therefore, we will drop the vector notation from here on.

2. *Gaussian beams and the Gauss-Laguerre modes*

a. General remarks. Under the experimental conditions which are most commonly encountered in laser physics—coaxial beams in cylindrical tubes—the use of cylinder coordinates is indicated. Let they be denoted by ρ,φ,ζ. The beam equation (15) takes the form (we delete the suffix T as we are dealing from here on exclusively with the transverse part of the field)

$$(\partial_\rho^2+\rho^{-1}\partial_\rho+\rho^{-2}\partial_\varphi+2i\partial_\xi)F=0 . \quad (16)$$

This equation is separable in either of the variables φ and ζ. If we separate the angular variable and use familiar arguments we find that solutions can be written as linear combinations

$$F(\rho,\varphi,\zeta)=\sum_m c_mG^m(\rho,\zeta)\exp(im\varphi) ,$$

where G^m satisfies

$$(\partial_\rho^2+\rho^{-1}\partial_\rho-m^2\rho^{-2}+2i\partial_\xi)G^m=0 ,$$

$$m=0,1,2,\ldots . \quad (17)$$

The solutions to the differential equation (17) are numbered by the integer m. For any given m, they have the following property which, in fact, is due to an internal symmetry of the equation: If $G^m(\rho,\zeta)$ is a solution to (17) and if a and b are complex constants (with $a\neq0$), then another solution is given by $G^m[a\rho,a^2(\zeta+b)]$, G^m being the same function as before.

b. Axial symmetry. Gaussian beams. The case of axial symmetry is given by $m=0$ and the beam equation reads simply

$$(\partial_\rho^2+\rho^{-1}\partial_\rho+2i\partial_\xi)G^0=0 . \quad (18)$$

We proceed to show how the "Gaussian beam" is obtained as a simple solution to this equation.

The symmetry of (17) just mentioned allows us to introduce a new coordinate $u:=\rho^2/\zeta$ to replace ρ. In the coordinates u,ζ, the differential equation takes the form

$$(4u\partial_u^2-2iu\partial_u+4\partial_u+2i\zeta\partial_\zeta)G^0=0 .$$

The separation ansatz $G^0(u,\zeta)=K(u)H(\zeta)$ yields the two equations (c is a complex constant, prime denotes differentiation in the respective variable)

$$4uK''-2iuK'+4K'+cK=0 , \quad (19)$$

$$2i\zeta H'-cH=0 . \quad (20)$$

The "simplest" choice for the constant is $c=-2i$, since in that case Eq. (19) will be satisfied by a function K which is a solution to the first-order differential equation

$$2K'-iK=0 ,$$

while (20) becomes

$$H'+\frac{1}{\zeta}H=0 .$$

Disregarding the trivial constants of integration we get

$$G^0=\frac{1}{\zeta}\exp(iu/2)=\frac{1}{\zeta}\exp(i\rho^2/2\zeta) . \quad (21)$$

Now, according to the remark made above, another solution to the beam equation is given by

$$G^0(\rho,\zeta)=\frac{1}{a^2(\zeta+b)}\exp[-\rho^2/2i(\zeta+b)] \quad (22)$$

where a and b are two complex constants. They will be determined by the following plausible requirements and conventions.

(i) For some value of ζ, the intensity $|F^0|^2$ has its maximum on the axis.

(ii) The origin of the ζ axis is placed at the location of the "beam waist," i.e., that point on the axis where the intensity is maximal.

(iii) At the origin of the coordinate system, the beam function G^0 takes the value 1, i.e., $G^0(0,0)=1$.

Using (22) one finds for the intensity

$$|G^0|^2=|a^2(\zeta+b)|^{-2}\exp\left[\frac{b^i\rho^2}{|\zeta+b|^2}\right], \quad (23)$$

where b^i is the imaginary part of b. Evidently, (i) implies $b^i<0$ which means that the intensity is Gaussian in any cross section $\zeta=$const. Next one looks up the minimum of the denominator in (23). With (ii) one finds that the real part of b vanishes, so that one may write $b=-i\beta$ with $\beta>0$. Finally, one considers (iii) which is merely another convention, fixing the arbitrary constant contained in F in such a way that $F=1$ at the position of the maximum of the intensity. This yields $a^2\beta=i$.

The beam function now becomes

$$F=\frac{2\beta}{2i\zeta+2\beta}\exp\left[\frac{-\rho^2}{2i\zeta+2\beta}\right] \quad (24)$$

and the dependence of the intensity on the radial coordinate is

$$|F|^2\sim\exp\left[\frac{-\beta\rho^2}{\zeta^2+\beta^2}\right].$$

Since the beam is Gaussian in any cross section $\zeta=$const, we may define a "scaled beam width" ρ_w as that value of ρ at which the intensity is e^{-2} times its value on the axis. It thus satisfies the condition

$$\frac{\beta\rho_w^2}{\zeta^2+\beta^2}=2$$

which is then solved to give

$$\rho_w(\zeta)=[2(\beta+\zeta^2/\beta)]^{1/2}. \quad (25)$$

We now remember that the characteristic length l_0, used in the scaling of coordinates, still remains to be chosen. So we impose on the scaled beam width the condition that it takes the value 1 at $\zeta=0$. It is then seen from (25) that $\beta=\frac{1}{2}$, so that for the beam function we get

$$F=\frac{1}{2i\zeta+1}\exp[-\rho^2/(2i\zeta+1)], \quad (26)$$

while (25) simplifies to

$$\rho_w(\zeta)=|1+2i\zeta|=(1+4\zeta^2)^{1/2}. \quad (27)$$

Equation (26) gives the Gaussian beam function in a handy and explicit manner in terms of the scaled coordinates.

The transition to the traditional form requires the return to the unscaled laboratory coordinates r and z.

In (25) we let $\rho_w(\zeta)$ correspond to the "beam width" $W(z)$, so that we have $\rho_w=W/l_0$. The condition $\rho_w(0)=1$ gives at once $W(0):=W_0=l_0$ which means that the beam width at the waist has been identified with the characteristic length. The parameter μ in (7) now becomes $\mu=c/\omega W_0$.

One thus finds the familiar expressions for the beam width,

$$W(z)=W_0[1+(2z/kW_0^2)^2]^{1/2},$$

and for the beam function,

$$F=\frac{q_0}{q}\exp(ikr^2/2q), \quad (28)$$

where $q:=z-ikW_0^2/2$ and $q_0:=q(0)$. The so-defined complex function $q(z)$ is referred to as the "complex curvature parameter" of the Gaussian beam, a nomenclature justified by the fact that the real part of $1/q$ does represent the real curvature of a wave front near the axis.

Other traditional forms of Eqs. (26) or (28) are obtained by writing $q(0)/q(z)$ either as $\exp[-iP(z)]$ or as $(W_0/W)\exp(-i\theta)$.

For convenience, we list some of the frequently used quantities as functions of the scaled length ζ:

$$q/q_0=1+2i\zeta,\quad (W/W_0)^2=1+4\zeta^2,$$
$$kW_0^2/q=2i/(1+2i\zeta).$$

Equation (28) or any of its numerous equivalent forms represent the "fundamental mode" of a Gaussian beam. Higher modes will be described in the next section.

c. Gauss-Laguerre modes. The task of solving the beam equation (17) under specified physical conditions is greatly simplified by the fact that it can be reduced to a well-known ordinary differential equation as follows.

Let $L_p^m(X)$ be a solution to the "associated Laguerre equation"

$$XL''+(m+1-X)L'+pL=0, \quad (29)$$

where m is an integer and p is a real constant. Then the complex function

$$G_p^m(\rho,\zeta):=C\frac{(1-2i\zeta)^{m/2+p}}{(1+2i\zeta)^{m/2+p+1}}X^{m/2}L_p^m(X)\times\exp[-X(1-2i\zeta)/2] \quad (30)$$

with

$$X:=2\rho^2/(1+4\zeta^2)$$

satisfies the beam equation (17). C is an arbitrary constant.

Since we are interested only in those solutions G which are regular on the axis $\rho=0$, we accept only those functions $L(X)$ which can be represented by power series. And since we exclude solutions which

diverge for $\rho \to \infty$, we admit only integer values of the parameter p (the other ones would give rise to divergent solutions). With that the power series breaks off at the term of order p, and the solution is an "associated Laguerre polynomial" L_p^m. We recall the Rodrigues formula (see, for example, Ref. 15)

$$L_p^m = \frac{1}{p!} e^X X^{-m} \frac{d^p}{dX^p} (e^{-X} X^{m+p}) .$$

Now the function G_p^m as given by (30) will be orthonormalized in the (r,φ) plane by taking

$$C = \frac{1}{W_0} \left[\frac{2p!}{\pi (p+m)!} \right]^{1/2} , \tag{31}$$

i.e., for any value of m it holds that (an asterisk represents the complex conjugate)

$$\int G_p^m G_q^{m*} r\, dr\, d\varphi = W_0^2 \int G_p^m G_q^{m*} \rho\, d\rho\, d\varphi = \delta_{pq} .$$

A function $f(\rho,\zeta)$ can be developed into a series (with fixed m)

$$f(\rho,\zeta) = \sum_p c_p^m(\zeta) G_p^m(\rho,\zeta)$$

whose coefficients are given by

$$c_p^m(\zeta) = 2\pi W_0^2 \int f(\rho,\zeta) G_p^{m*}(\rho,\zeta) \rho\, d\rho .$$

In the case where $f(\rho,\zeta)$ is a beam function [i.e., satisfies (17)] the coefficients c_p^m are independent of ζ. It is this property of the G_p^m which makes them useful in the treatment of laser beams.

The functions G_p^m are said to describe the "Gauss-Laguerre modes" of the laser beam. Under most experimental conditions the beam has axial symmetry, a case which corresponds to setting $m=0$. Formulas (30) and (31) then specialize to (we omit the superscript index zero)

$$G_p(\rho,\zeta) = \left[\frac{2}{\pi} \right]^{1/2} W_0^{-1} \frac{(1-2i\zeta)^p}{(1+2i\zeta)^{p+1}} \times L_p(X) \exp[-X(1-2i\zeta)/2] . \tag{32}$$

Note that the lowest-order mode G_0 is the fundamental mode F given by (26). The two formulas differ only by the normalization factor $\sqrt{2/\pi} W_0^{-1}$.

As the axially symmetric Gauss-Laguerre modes are widely used, we give also their more familiar form in terms of the beam parameters and in unscaled coordinates (with W,q,θ given at the end of Sec. I A 2 b)

$$G_p(r,z) = \left[\frac{2}{\pi} \right]^{1/2} W(z)^{-1} \exp(ikr^2/2q) \times \exp[-i(2p+1)\theta] L_p(X) .$$

d. Backward beams. Up to here the description of beams has been given with the tacit understanding that they propagate in the positive z direction. In discussing laser resonators it is useful to distinguish between the fields which propagate in the forward $(+z)$ direction and in the backward $(-z)$ direction.

There is no difficulty in representing the two kinds of beams. In Eq. (5) a positive k means a forward beam and a negative k means a backward beam. With the introduction of scaled coordinates, however, the quantity $|k|$ has been absorbed into ζ and has thus disappeared from the equations. But it is clear that in order to pass from a forward to a backward beam all one has to do is to change the sign of ζ in the equations. For the Gauss-Laguerre modes this simply means to replace the beam function by its complex conjugate.

3. *The transverse resonance condition*

To have something specific in mind, let us consider the "quasihemispheric cavity" (Fig. 1), i.e., a type quite often used in laser physics. It has a plane mirror (which we put to the left, at $z=0$) and a concave mirror (with radius of curvature R) at a distance d to the right. The diameters of the mirrors are much larger than the beam width, i.e., at present we disregard possible diffraction effects.

When a cavity is brought to resonate one finds in it a mixture of different modes which all belong to the same curvature q. The latter is determined by the position of the beam waist and by the "spot size" W_0. In the assumed configuration the beam waist is at the position of the flat mirror. W_0 can be obtained in terms of the parameters R and d:

$$W_0^2 = \frac{\lambda}{\pi} \sqrt{d(R-d)} . \tag{33}$$

This formula can be derived by means of the "transverse resonance condition" which states that in the case of resonance the curvature of any wave front is preserved after a round trip.

The familiar formula for the change of curvature of a spherical wave front and the conservation of beam waists under reflection lead to (the indices f and b refer to the forward and the backward beam)

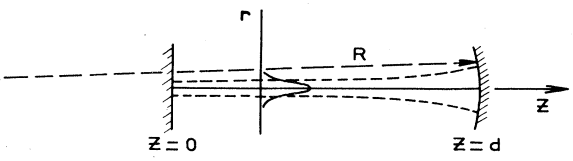

FIG. 1. Laser geometry, schematic.

$$\frac{1}{q_f}+\frac{1}{q_b}=0 \text{ at } z=0 ,$$
$$\frac{1}{q_f}+\frac{1}{q_b}=\frac{2}{R} \text{ at } z=d .$$

These two equations, together with $q_f(d)=q_f(0)+d$ and $q_b(d)=q_b(0)+d$ give formula (33).

B. The cavity with an amplifying medium

1. *The inhomogeneous medium*

The confinement of an amplifying medium in a tube results in a nonuniform distribution of the laser-active atoms. This inhomogeneity has been observed as well in a HeNe laser[16] as in a high-gain Xenon laser[17] at 3.5μ. In both cases it was found that the gain was maximal on the axis as long as the currents were kept sufficiently weak, but that the opposite was true for stronger currents.

We will describe the density of active atoms by a parabolic approximation of the form $N_0(1-u\rho^2)$, where u is an adjustable parameter. According to the experiment just mentioned u can take a negative value in a high-gain laser with a strong current, but in that case, the parabolic approximation is often not sufficient, especially in the case of a high-gain laser with plane mirrors.

Now, in accordance with a previous calculation using plane waves,[18] we assume the following expressions for the polarizabilities at a point (ρ,ζ). For a forward wave,

$$\alpha_f(\rho,\zeta)=[\alpha_0+\beta_1|E_f(\rho,\zeta)|^2+\beta_2|E_b(\rho,\zeta)|^2](1-u\rho^2) ; \tag{34a}$$

for a backward wave,

$$\alpha_b(\rho,\zeta)=[\alpha_0+\beta_2|E_f(\rho,\zeta)|^2+\beta_1|E_b(\rho,\zeta)|^2](1-u\rho^2) . \tag{34b}$$

Expressions for the complex quantities α_0, β_1, and β_2 can be found in Ref. 18 (where β_1 and β_2 had been named α_1 and α_2).

In the above formulas, the "forward" and the "backward" fields have been separated since they have quite different amplitudes, as we will see later. The coefficient β_1 takes care of the self-saturation of a wave, whereas β_2 is responsible for the saturation by an oncoming wave, a phenomenon from which the Lamb dip originates.

The description of the saturated medium has been simplified since, e.g., neither the spatial harmonics (saturation gratings) nor the variation of the collision parameters as a function of intensity have been taken into account. The analysis of the parameters β_1 and β_2 reveal the form of the sub-Doppler line.[19] Furthermore, we are approximating the saturation term by a quadratic expression, e.g., for the forward wave

$$(1-u\rho^2)|E_f(\rho,\zeta)|^2=(1-u\rho^2)|E_f(0,\zeta)|^2\exp\left[-2\frac{W_0^2}{W^2}\rho^2\right]=:(1-A\rho^2)|E_f(0,\zeta)|^2 .$$

The interpolating function $A(\zeta)$ will be determined in such a way that the two expressions on the right equal each other on a coaxial surface given by $W_0\rho/W=\tilde{\rho}$, where $\tilde{\rho}$ is a constant which has to be given.

This procedure results in the formula

$$A(\zeta)=\frac{W_0^2}{W^2\tilde{\rho}^2}+\left[u-\frac{W_0^2}{W^2\tilde{\rho}^2}\right]\exp(-2\tilde{\rho}^2) . \tag{35}$$

We emphasize that the parabolic approximation is not a Taylor expansion in ρ^2. Rather we are introducing an interpolating function A to represent that part of the lens effect which is due to saturation. It is important to note that A must be a function of ζ in order to assure the same approximation all along the laser axis.

The equations to be solved are (11) and (12) with their counterparts for the backward wave. In their right-hand sides we need the expressions α_{nf} and α_{nb} for the nonuniform parts of the polarizability of the forward and the backward wave. According to (34) and (35) we can write

$$\alpha_{nf}=\epsilon_0 T_f(\zeta)-\rho^2[u\alpha_0+A\epsilon_0 T_f(\zeta)] , \tag{36a}$$
$$\alpha_{nb}=\epsilon_0 T_b(\zeta)-\rho^2[u\alpha_0+A\epsilon_0 T_b(\zeta)] , \tag{36b}$$

where we have introduced the auxiliary functions of a single variable

$$T_f(\zeta):=\frac{\beta_1}{\epsilon_0}|E_f(0,\zeta)|^2+\frac{\beta_2}{\epsilon_0}|E_b(0,\zeta)|^2 , \tag{37a}$$
$$T_b(\zeta):=\frac{\beta_2}{\epsilon_0}|E_f(0,\zeta)|^2+\frac{\beta_1}{\epsilon_0}|E_b(0,\zeta)|^2 . \tag{37b}$$

We then get the following equations for the transverse and the longitudinal field components of the forward wave (we delete here the subscript f to unclutter the notation):

$$-\nabla_T(\mu\nabla_T F_T+\mu^2\partial_\zeta F_\zeta+iF_\zeta)+\mu\nabla_T^2 F_T+\mu^3\partial_\zeta^2 F_T+2i\mu\partial_\zeta F_T=-\mu^{-1}\frac{\alpha_{nf}}{\epsilon_0}F_T , \tag{38}$$

$$-\mu^3\partial_\zeta(\nabla_T F_T)-i\mu\nabla_T F_T+\mu^2\nabla_T^2 F_\zeta = -\left[1+\frac{\alpha_f}{\epsilon_0}\right]F_\zeta \,. \quad (39)$$

Similar equations hold for the backward field.

The equations are to be considered within the framework of the paraxial approximation. The reasoning is similar to that of Sec. I A 1, and we conclude as before that F_ζ is of order one in the development parameter μ.

However, we now relax the smallness condition on α_n/ϵ_0 and require only that it is of order two in μ (and not, as assumed in Sec. I A 1, of order three), or even greater than that. For instance, in the case of a HeNe gas laser working at 3.39μ the order of magnitude is 5×10^{-4} for μ, and 5×10^{-6} for α_0/ϵ_0.

With that assumption, Eqs. (38) and (39) give the following in lowest order (as only transversal components of order zero enter the equations, we delete the subscript T and the superscript zero in the beam function). For a forward wave

$$\nabla_T^2 F_f(\rho,\zeta)+2i\partial_\zeta F_f(\rho,\zeta)=-\frac{\omega^2}{c^2}W_0^2\left[T_f(\zeta)-\rho^2\left[\frac{\alpha_0}{\epsilon_0}u+AT_f(\zeta)\right]\right]F_f(\rho,\zeta)\,, \quad (40)$$

for a backward wave

$$\nabla_T^2 F_b(\rho,\zeta)-2i\partial_\zeta F_b(\rho,\zeta)=-\frac{\omega^2}{c^2}W_0^2\left[T_b(\zeta)-\rho^2\left[\frac{\alpha_0}{\epsilon_0}u+AT_b(\zeta)\right]\right]F_b(\rho,\zeta)\,. \quad (41)$$

The first term in the square bracket on the right-hand side corresponds to the case of a homogeneous medium while the second one, due to its dependence on the radial coordinate, describes the lens effects.

Notice that, for positive u, the lens effect due to saturation (proportional to β_1,β_2) is opposite to the one due to the distribution of atoms (proportional to α_0). These effects are illustrated in Fig. 2.

2. *The inhomogeneous beam equation*

Despite all previous simplifications (40) and (41) still constitute a coupled system of nonlinear partial differential equations. The problem of solving this system is greatly facilitated by the fact that a suitable substitution converts it into a system of ordinary differential equations.

We write for the forward and the backward beam

$$F_f(\rho,\zeta)=F_{0f}(\rho,\zeta)\exp\left[-i\left[\epsilon_f-\frac{\rho^2}{2}\eta_f\right]\right], \quad (42a)$$

$$F_b(\rho,\zeta)=F_{0b}(\rho,\zeta)\exp\left[-i\left[\epsilon_b+\frac{\rho^2}{2}\eta_b\right]\right], \quad (42b)$$

where F_{0f} and F_{0b} are Gaussian beam functions [satisfying (40) and (41) with vanishing right-hand side] and where ϵ_f, η_f, ϵ_b, and η_b are (as yet undetermined) complex functions depending on the real variable ζ.

The approach is based upon the idea[11] that the presence of an amplifying medium results in a modification of the Gaussian mode which was found in the empty cavity.

ϵ_f represents the modification of the longitudinal part (phase and amplitude) of the field, while $\frac{1}{2}\eta_f$ describes the modification of the transverse part (complex curvature, i.e., R and W). The new transverse parameter is then

$$\frac{1}{q_f}+\frac{c}{\omega W_0^2}\eta_f=\frac{1}{R}+2i\frac{c}{\omega}\frac{1}{W^2}+\frac{c}{\omega W_0^2}\eta_f^r+i\frac{c}{\omega W_0^2}\eta_f^i\,.$$

It is seen that η_f^i and η_f^r describe, respectively, the modification of the beam diameter and the radius of

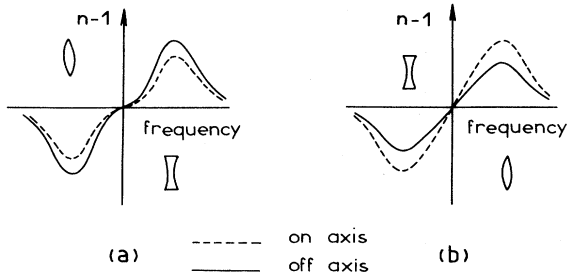

FIG. 2. Lens effects due to the inhomogeneity of (a) the saturation and (b) the distribution of amplifying atoms. (a) On the high-frequency side, $|n-1|$ increases away from the axis, causing the optical length to be greater in the outer regions. This amounts to the action of a diverging lens. For low frequencies one finds the contrary. (b) The number of amplifying atoms decreases away from the axis, resulting in a lower value of $|n-1|$ in the outer regions. This amounts to the action of a converging (diverging) lens on the high- (low-) frequency side, giving lens effects opposite to those of (a).

curvature due to the lens effects and are dependent on frequency. Previously, the modifications had been termed "R effect" and "W effect."[12]

When (42) is inserted into (40) one finds for the two beams the ordinary differential equations

$$\epsilon_f' + i\eta_f = -\frac{1}{2}\frac{\omega^2}{c^2} W_0^2 T_f \,, \tag{43a}$$

$$\epsilon_b' + i\eta_b = \frac{1}{2}\frac{\omega^2}{c^2} W_0^2 T_b \,, \tag{43b}$$

$$\eta_f' + \frac{4i}{1+2i\zeta}\eta_f + \eta_f^2 = -\frac{\omega^2}{c^2} W_0^2 \left[\frac{\alpha_0}{\epsilon_0} u + A T_f\right], \tag{44a}$$

$$\eta_b' - \frac{4i}{1-2i\zeta}\eta_b + \eta_b^2 = -\frac{\omega^2}{c^2} W_0^2 \left[\frac{\alpha_0}{\epsilon_0} u + A T_b\right]. \tag{44b}$$

Equations (44) describe the evolution of the transverse parameters η_f, η_b along the axis. For an optically thin medium, the case we are interested in, η^2 is much smaller than η and can, therefore, be neglected. The equations are still nonlinear and they are coupled via the functions T.

Approximate solutions of these equations in the case $u=0$ and $\tilde{\rho}=1$ show[11] that self-focusing and self-defocusing effects depend on properties of the medium and on boundary conditions. Properties of the medium are reflected in η_f^i by a dispersion-shaped function and in η_f^r by a symmetrical function of frequency. Boundary conditions influence these quantities much less, but it is important to note that they give rise to an asymmetric part of the function η_f^r. The reason for the importance of this fact is explained by Eq. (43) which expresses ϵ_f' as a function of η_f and T_f. Remarking that $\epsilon_f'^i$ is that part of the differential gain which describes saturation, we see that $\epsilon_f'^i$ depends on η_f^r and T_f^i. Now, the nonsymmetrical function appearing in η_f^r will give rise to a nonsymmetrical saturation curve and this, in turn, will result in an asymmetrical line shape. We have experimentally verified this prediction[12] at 3.39μ using a segmented tube working at a high current in order to decrease the inhomogeneity in the distribution of atoms. In that paper, evidence has been given that the R effect and the "Garside effect"[7] add together to give an asymmetry such that the maximum of intensity is on the low-frequency side of the line. This can be measured using a small area detector near the mirror on the laser axis. If the total output energy of the laser is measured with a large area detector, this asymmetry is considerably decreased by the W effect which almost cancels the R effect. What remains is essentially the Garside effect, nicely observed in a recent experiment.[8] In the present work we will use (43) and (44) together with a simplified expression for the field amplitude in order to compute the z dependence of various relevant variables.

II. THEORY OF A DIAPHRAGMED LASER WITH AN AMPLIFYING INHOMOGENEOUS MEDIUM

A. Resonant field distribution in an empty diaphragmed cavity

In order to assure the single-mode operation of a laser it is necessary to suppress the Gauss-Laguerre modes of higher order, i.e., for m and $p \neq 0$. Experimentally this is achieved by placing a diaphragm inside the cavity. It causes increased losses for the higher modes simply because it limits the spreading of the beam. However, the modes themselves are changed by the diffraction effects induced by the diaphragm. Every new mode is characterized by its own proper amplitude and phase distribution. An appropriate means for their description are the Gauss-Laguerre modes and it is the aim of this section to develop the corresponding method of calculation.

We first consider an empty cavity with the diaphragm at the location of the concave mirror (Fig. 3). As the cavity is axially symmetric we are dealing with beams having axial symmetry. Thus, any field inside the cavity can be decomposed with respect to Gauss-Laguerre modes G_p $(:=G_p^0)$.

In order to formulate the resonance condition we need the notion of the "round-trip operator" $\mathcal{R}$. Consider the changes a wave front undergoes during a round trip inside the cavity: A phase change at every reflection by a mirror, a change of curvature upon reflection by the concave mirror, and the diffraction by the diaphragm. The round-trip operator summarizes the changes of the field during a round trip by giving the final field in terms of the initial field. The resonance condition will, of course, state that the proper wave mode does not change during a round trip, in other words, that it is an eigenvector

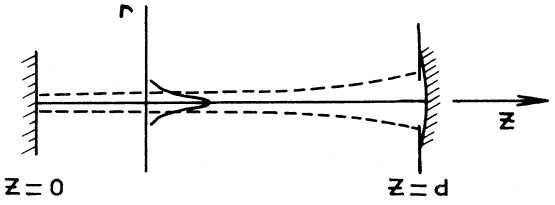

FIG. 3. Diaphragmed laser.

of the round-trip operator.

As before, we use the indices f and b to distinguish between the forward and the backward field. The concave mirror is at $z=d$, the radius of the diaphragm is denoted by b. The reflectances are denoted r_A for the plane and r_B for the concave mirror. We write the equations of this paragraph in the coordinates r,z.

Let the field at the position of the mirrors be given by the following expressions:

$$F_f(r,0)=\sum_p f_p G_{fp}(r,0)\ ,$$
$$F_b(r,0)=\sum_p b_p G_{bp}(r,0)\ , \tag{45a}$$
$$F_f(r,d)=\sum_p f_p G_{fp}(r,d)\ ,$$
$$F_b(r,d)=\sum_p b_p G_{bp}(r,d)\ . \tag{45b}$$

The conditions imposed on the field by the diaphragm are

$$F_b(r,d)=\begin{cases} r_B F_f(r,d) & \text{for } r<b \\ 0 & \text{for } r>b\ . \end{cases} \tag{46}$$

Equation (45) allows one to calculate the coefficients

$$b_p=\int F_b(r,d)G^*_{bp}(r,d)ds$$

as integrals over the infinite surface $z=d$. Using (46) we get

$$b_p=2\pi r_B\int_0^b r\,dr\,F_f(r,d)G^*_{bp}(r,d)$$
$$=2\pi r_B\int_0^b r\,dr\sum_q f_q G_{fq}(r,d)G^*_{bp}(r,d)\ .$$

Defining the symmetric matrix elements

$$\Lambda_{pq}=\exp[-2i(p+q)\theta_d]\int_0^{X_b} e^{-X}L_p(X)L_q(X)dX$$

we can write

$$b_p=r_B\exp(2ikd-2i\theta_d)\sum_q \Lambda_{pq}f_q\ .$$

We recall the formulas $\theta_d=\arctan\sqrt{(R-d)d}$ and $X_b:=2b^2/W_d^2$, where $W_d:=W(d)=W_0\sqrt{R/(R-d)}$.

At the plane mirror, the condition of reflection is $r_A b_p=f_p$. Thus, a field of the form (45) and reflected by the plane mirror will be transformed into a field $\sum_p f'_p G_{fp}(r,0)$ with

$$f'_p=r_A r_B\exp(2ikd-2i\theta_d)\sum_q \Lambda_{pq}f_q\ .$$

As the resonance condition states that after a round trip $f'_p=\lambda f_p$ holds for all p, we get for the elements of the round-trip operator

$$\mathscr{R}_{pq}=r_A r_B\exp(2ikd-2i\theta_d)\Lambda_{pq}\ . \tag{47}$$

The proper modes of the cavity are the eigenvectors of this operator. They are complex since the operator is complex. The same holds true for the eigenvalues each of which is then characterized by an amplitude (absolute value) and by a phase.

The eigenvector belonging to the "largest" eigenvalue can be found by the iteration method of Caulfield *et al.*[20] As the diameter of the diaphragm is increased, this vector approaches the fundamental Gaussian mode and in that sense it may be regarded as the fundamental mode of the diaphragmed cavity. The following treatment is concerned with this fundamental mode.

After having determined the coefficients f_p one can also compute the b_p and thus obtain the intensity distribution for the field corresponding to the fundamental mode. Figure 4 shows various intensity distributions which have been calculated for demonstration purposes. The calculation of the field was done under the assumption that during a round trip the losses were completely compensated by the amplifying medium whose gain was taken to be constant inside the tube. In Fig. 4(b) one notices that the maximum of the intensity is not at the position of the plane mirror, but occurs in the backward

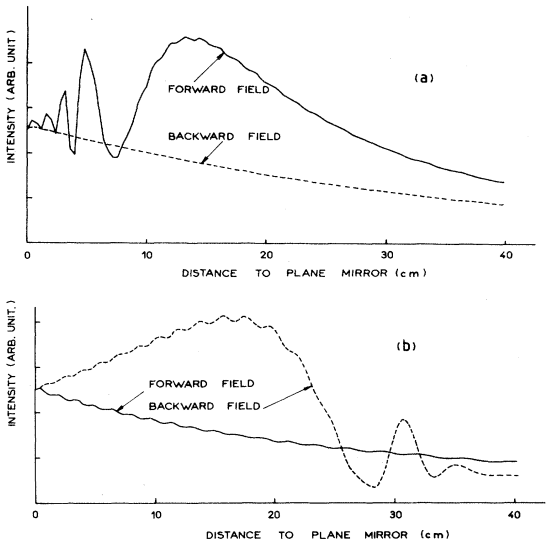

FIG. 4. Resonant diffracted field distribution along the laser axis with the diaphragm (a) on the plane mirror, (b) on the concave mirror. Curves were calculated through the use of (a) 100 Laguerre polynomials, (b) 60 polynomials. We have noted that the greater the number of polynomials, the better the definition of the curves. Step width in the calculation is 4 mm, corresponding to 100 steps along the length of the laser. These curves are comparable to those obtained in the study of diffraction phenomena outside a resonant cavity (Ref. 21).

beam which also contains other oscillations due to diffraction. In contrast, the forward beam shows a more regular behavior. The curves exhibit the familiar features of light diffracted by a circular aperture.[21] One also notices that the converging power of the diaphragm is added to that of the concave mirror, a fact which explains the shift of the maximum of intensity to the right. Similarly, Fig. 4(a) shows the distribution of intensity, calculated by the same method as before, in the case where the diaphragm is at the plane mirror. Here, the maximum of intensity appears on the forward beam, giving a diffraction figure which is different from the previous one.

B. Diffraction effects in a gas laser. Numerical calculation

We consider a diaphragmed laser with axially symmetric geometry and an axially symmetric intensity distribution in it. The fields are written as a superposition of Gauss-Laguerre modes:

$$F_f(\rho,\zeta)=\sum_p f_p G_{fp}(\rho,\zeta)\exp[-i(\epsilon_{fp}-\tfrac{1}{2}\rho^2\eta_{fp})] , \tag{48a}$$

$$F_b(\rho,\zeta)=\sum_p b_p G_{bp}(\rho,\zeta)\exp[-i(\epsilon_{bp}+\tfrac{1}{2}\rho^2\eta_{bp})] . \tag{48b}$$

The complex functions $\epsilon_{fp}(\zeta)$, $\eta_{fp}(\zeta)$, $\epsilon_{bp}(\zeta)$, and $\eta_{bp}(\zeta)$ represent the change of a mode p due to the laser action. The coefficients f_p and b_p are obtained from the resonant field of the empty cavity and are, therefore, independent of the coordinates. Equations (48) thus generalizes (42) which applies to the case $p=0$. We will use (48) as an ansatz for the numerical solution of the basic equations (40) and (41).

So, we insert (48) into Eqs. (40) and (41) and consider the resulting equations. After some algebra we find for their left-hand side

$$\left[\partial_\rho^2+\frac{1}{\rho}\partial_\rho+2i\partial_\zeta\right]F_f(\rho,\zeta)=\sum_p f_p G_{fp}(\rho,\zeta)\exp[-i(\epsilon_{fp}-\tfrac{1}{2}\rho^2\eta_{fp})]$$
$$\times\left[2(\epsilon'_{fp}+i\eta_{fp})-\rho^2\left[\eta'_{fp}+\frac{4i}{1+2i\zeta}\eta_{fp}+\eta_{fp}^2\right]+4ip\left[1-\frac{L_{p-1}}{L_p}\right]\eta_{fp}\right] . \tag{49}$$

A similar equation would have to be written for the backward field. Evidently, the last term in the large square brackets vanishes when p is zero, giving back the terms on the left-hand side of Eqs. (43) and (44). Also, for small values of ρ, the term behaves as ρ^2. If the term would be neglected, the equations would be decomposable into a set of pairs of equations identical to the pair (43) and (44). On the other hand, if the term is retained, the splitting of the equations into terms which are either independent of ρ or proportional to ρ^2 would be impossible and the advantage of the method would be lost.

Physically, the term in question is responsible for the variation of the figure of diffraction with frequency. Since the medium is optically thin and, consequently, that variation is small, we will drop the term from the equations. Moreover, we will assume that the active medium will change each mode in the same way. This amounts to assuming that $\epsilon_{fp}\approx\epsilon_f$ and $\eta_{fp}\approx\eta_f$ for all p, and similarly for the backward beam.

We now can write (48) in the form

$$F_f(\rho,\zeta)=\exp[-i(\epsilon_f-\tfrac{1}{2}\rho^2\eta_f)]\sum_p f_p G_{fp}(\rho,\zeta) , \tag{50a}$$

$$F_b(\rho,\zeta)=\exp[-i(\epsilon_b+\tfrac{1}{2}\rho^2\eta_b)]\sum_p b_p G_{bp}(\rho,\zeta) . \tag{50b}$$

The expressions for the fields $E_f(0,z)$ and $E_b(0,z)$ needed on the right-hand sides of (43) and (44) then take the form

$$E_f(0,z)=E_f e^{i(kz-\omega t)}F_f(0,z)$$
$$=E_f\exp[i(kz-\omega t)-i\epsilon_f]V_f(z) , \tag{51a}$$

$$E_b(0,z)=E_b e^{i(-kz-\omega t)}F_f(0,z)$$
$$=E_b\exp[i(-kz-\omega t)-i\epsilon_b]V_b(z) , \tag{51b}$$

where E_f and E_b are constants and where we have defined

$$V_f(z):=\sum_p f_p G_{fp}(0,z) ,$$

$$V_b(z):=\sum_p b_b G_{bp}(0,z) .$$

From Eqs. (43) and (51a) we obtain the following difference equations (dz is the step size to be chosen for the integration):

$$|E_f(0,z+dz)|^2$$
$$=|E_f(0,z)|^2\left|\frac{V_f(z+dz)}{V_f(z)}\right|^2$$
$$\times\exp\left[-2dz\left[k^i+\frac{c}{\omega}\frac{\eta_f^r}{W_0^2}+\frac{\omega}{2c}T_f^i\right]\right] , \tag{52a}$$

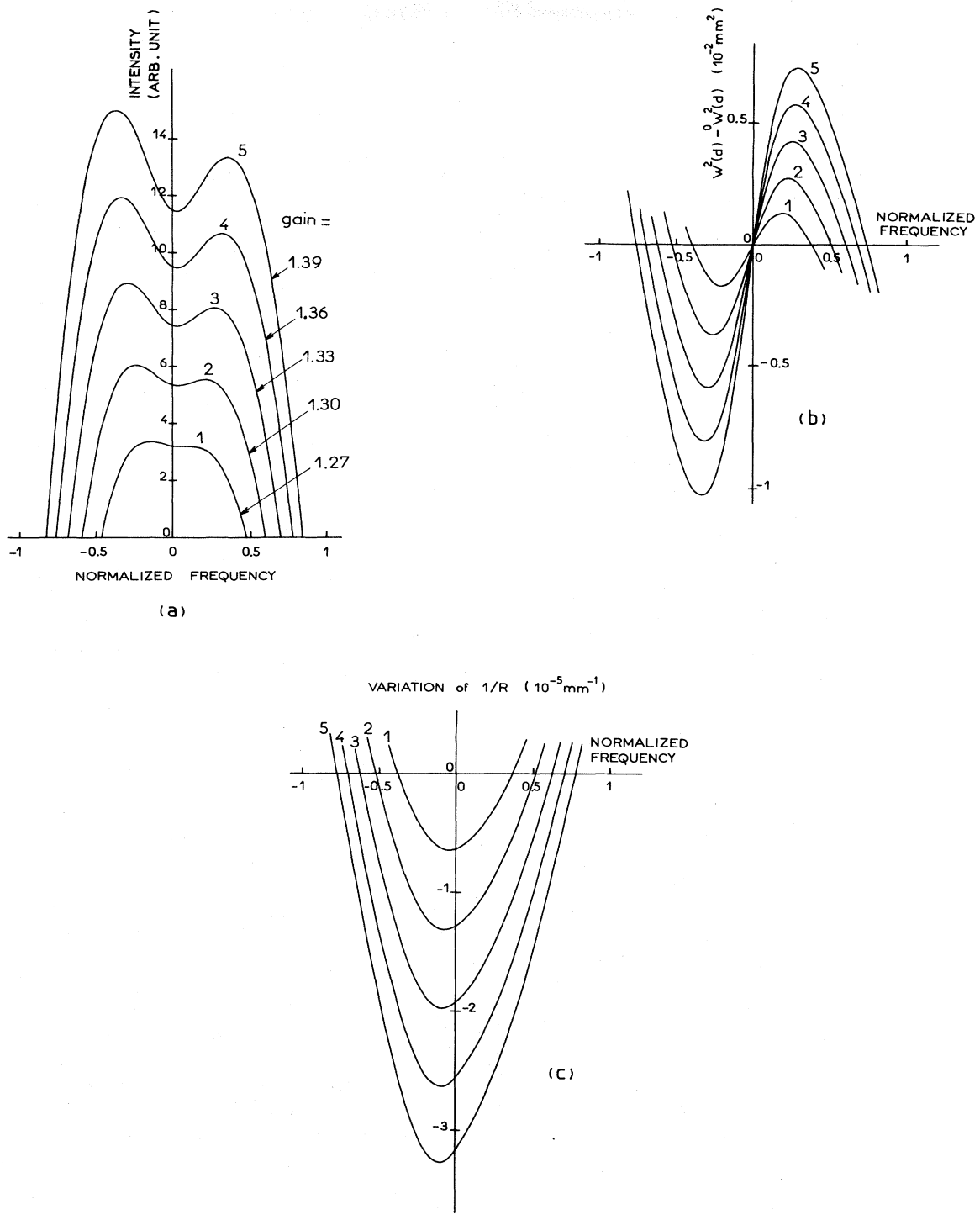

FIG. 5. (a) Intensity on the laser axis, (b) variation of beam surface, (c) variation of its radius of curvature at $z=d$ vs reduced frequency $(\omega-\omega_0)/kv_M$. Curves were obtained for a weak atom inhomogeneity ($u=W_0^2/4$) and the following parameters. Concave mirror: radius of curvature 600 mm, reflectivity 0.8. Plane mirror: reflectivity 1, laser length 400 mm, diameter of the diaphragm 2.6 mm. Amplifying medium fills the cavity. Asymmetry of the curve is fixed here by the inhomogeneity of saturation (i.e., by the self-focusing and defocusing effects). Because of the weakness of the population inhomogeneity, we find here the same line shapes as previously published (Ref. 11) in the case of a homogeneous medium. These line shapes are observable with a small area detector (Ref. 11).

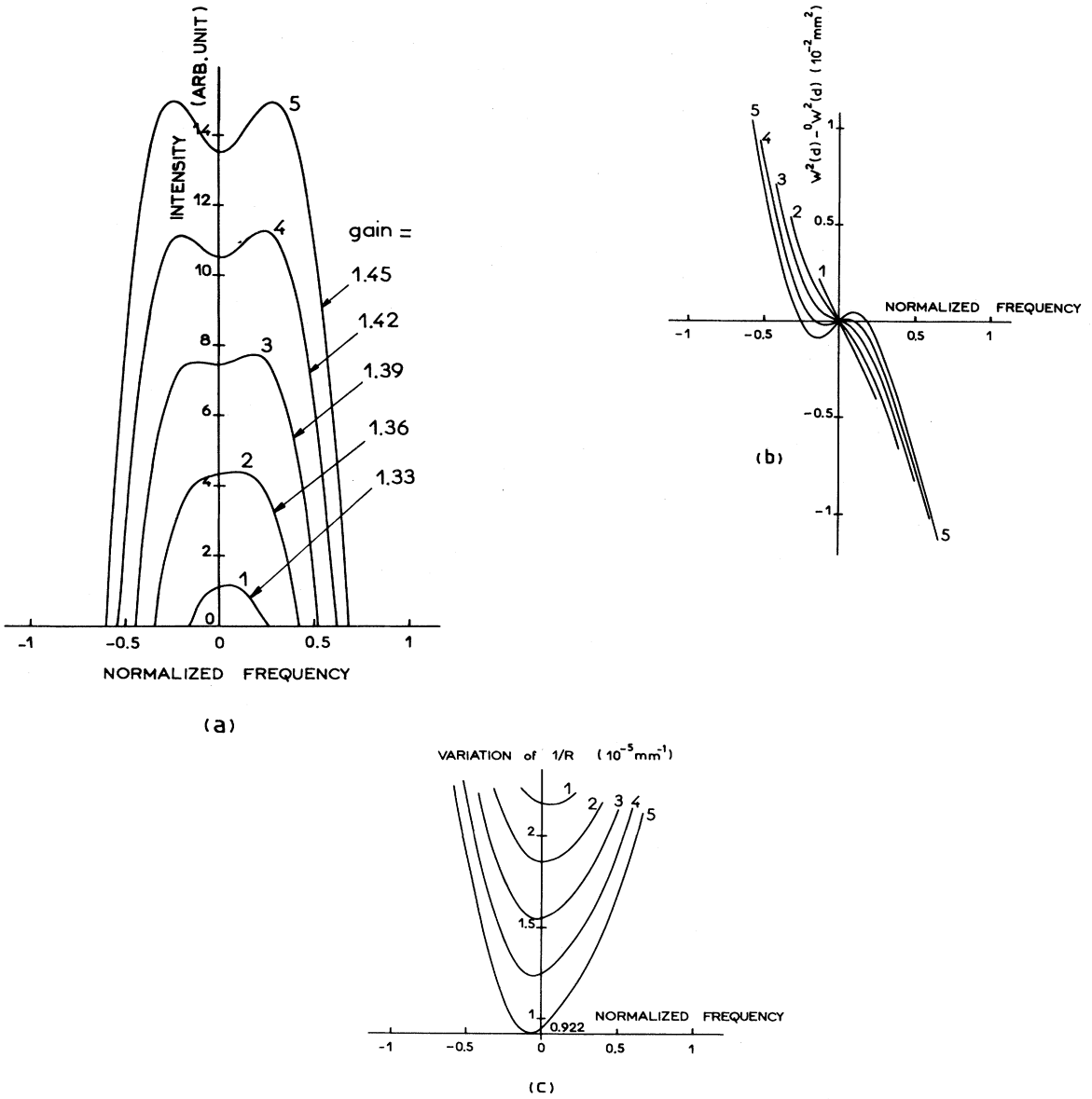

FIG. 6. Same quantities as in Fig. 5, but with $u = W_0^2/0.81$. For this value of u, the competition between the two effects which determine the asymmetry of the line shape [Fig. 6(a)] is shown by a decrease of the asymmetry for increasing gain. For weak gain, the intensity is weak and the population effects give a maximum on the right. For the higher gain, saturation effects have increased sufficiently to almost compensate the population effects. This evolution is also clearly shown on Fig. 6(c). Comparison between Figs. 5(c) and 6(c) show that inhomogeneity of saturation has the tendency to diminish η_a^i: As η_a^i decreases, the intensity increases. Population inhomogeneity has the inverse effect, i.e., it pushes the curves up.

$$|E_b(0,z+dz)|^2 = |E_b(0,z)|^2 \left| \frac{V_b(z+dz)}{V_b(z)} \right|^2 \times \exp\left[-2dz \left[-k^i + \frac{c}{\omega} \frac{\eta_b^r}{W_0^2} - \frac{\omega}{2c} T_b^i \right] \right] . \quad (52b)$$

Here, the superscripts r and i indicate the real and imaginary part of the quantity respectively. From (44) we obtain the equations (we neglect $\eta_{f,b}^2$)

$$\eta_f(z+dz) = \eta_f(z) - dz \left[2\frac{\eta_f}{q_f} + \frac{\omega}{c} \left[\frac{\alpha_0}{\epsilon_0} u + A T_f \right] \right] , \quad (53a)$$

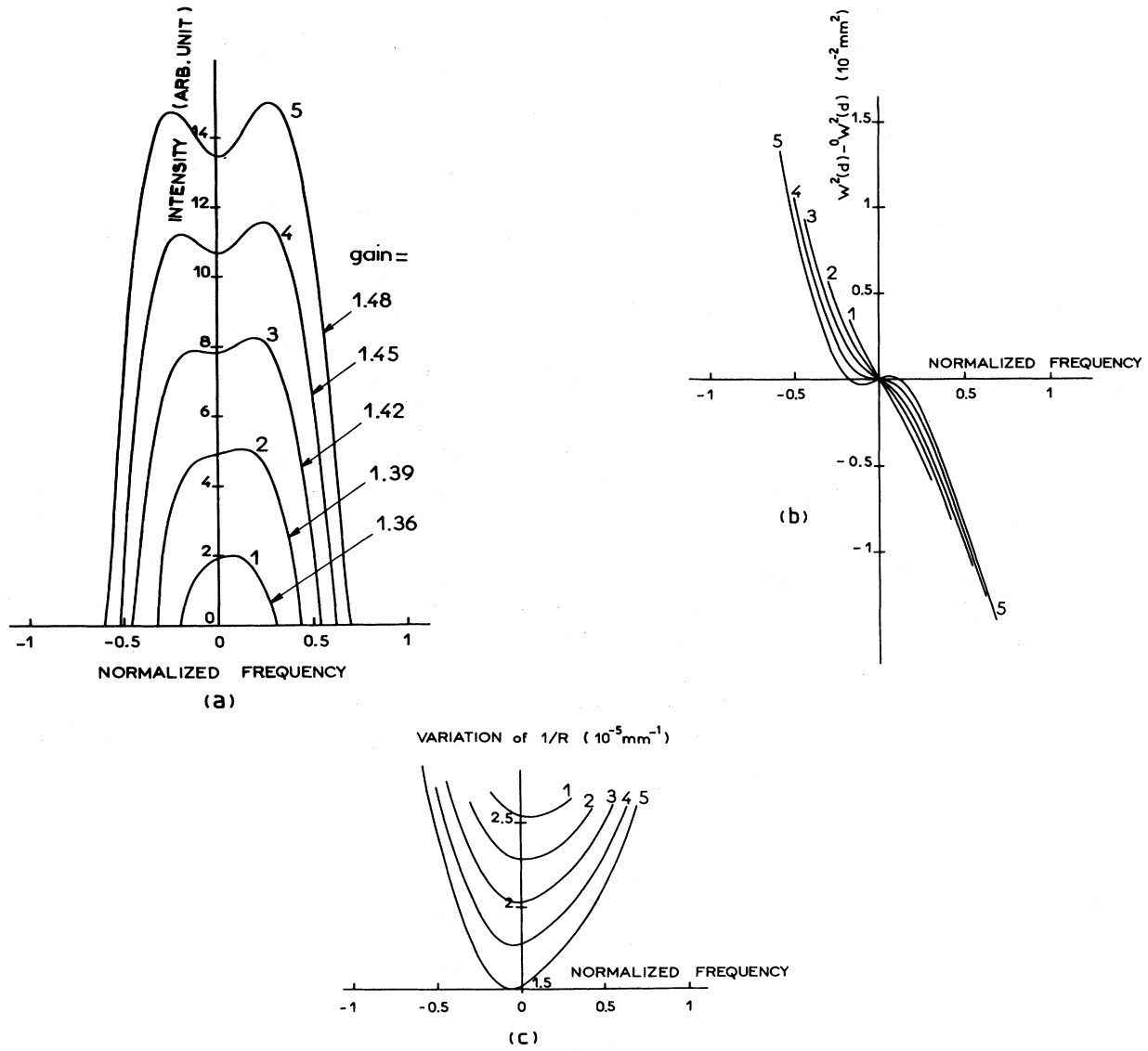

FIG. 7. Same quantities as in Figs. 5 and 6, but with $u = W_0^2/(0.85)^2$. This time, the leading effect which fixes the asymmetry of the line [Fig. 7(a)] is the inhomogeneity of the distribution of active atoms, and the maximum of the intensity is always on the high-frequency side. Noticeable also is the large displacement of the curves towards the higher frequencies. Figure 7(c) shows an amplification of the effect commented on Fig. 6(c). Figure 7(b) shows that the variation of the mode surface is almost entirely determined by the population inhomogeneity leading to an evolution opposite to that shown in Fig. 5(b). Figures 5(b), 6(b), and 7(b) illustrate the influence of the increase of this inhomogeneity on the transversal mode surface.

$$\eta_b(z+dz)=\eta_b(z)-dz\left[2\frac{\eta_b}{q_b}+\frac{\omega}{c}\left[\frac{\alpha_0}{\epsilon_0}u+AT_b\right]\right]. \tag{53b}$$

The boundary conditions on the mirrors are (we are treating here the case where the diaphragm is at the concave mirror) at $z=d$:

$$|E_b(d)|^2=|r_B|^2|\lambda_p|^2|E_f(d)|^2,$$

$$\eta_f(d)=-\eta_b(d),$$

where λ_p is the eigenvalue of the resonant mode calculated for the ratio $b/W(d)$. Similarly, we get, at $z=0$,

$$|E_b(0)|^2=|r_A|^{-2}|E_f(0)|^2,$$

$$\eta_f(0)=-\eta_b(0).$$

Since $W(d)$ depends on the frequency, the eigenvalue λ_p and the first boundary condition are also frequency dependent.

The difficulty posed by the difference equations

and the boundary conditions lies in the fact that the latter depend on the solution itself, so that we are dealing with a self-consistency problem. We will attack that problem by using Newton's approximation method. It will be applied to find the zeros of the quantities

$$L:=|E_f(0)|^2/|E_b(0)|^2-|r_A|^2,$$

$$M:=\eta_f^i(0)+\eta_b^i(0),\quad N:=\eta_f^r(0)+\eta_b^r(0)$$

considered as functionals of the variables

$$X:=|E_f(d)|^2,\quad Y:=\eta_f^i(d),\quad Z:=\eta_f^r(d).$$

We are looking for those values X,Y,Z for which the functionals L,M,N vanish.

To determine a suitable starting point for the approximation we first calculate values X_1,Y_1,Z_1 by using a mean field (E_m) approximation[11] for the center of the line, getting

$$X_1=|E_m|^2=\frac{-(\alpha_0^i/\epsilon_0)+(\lambda/4\pi d)\ln(r_A r_B)}{(\beta_1^i+\beta_2^i)/\epsilon_0},$$

$$Y_1=0,$$

$$Z_1=-\tfrac{1}{4}AW_0^2T_f^i=-AW_0^2(\beta_1^i+\beta_2^i)|E_m|^2/4\epsilon_0.$$

Using Eqs. (52) and (53) we now find the values L_1,M_1,N_1 at $z=0$. In the next step we calculate L_2,M_2,N_2 at a point $X_2=X_1+dX, Y_2=Y_1, Z_2=Z_1$. This gives the partial difference quotients

$$\partial L/\partial X=(L_2-L_1)/(X_2-X_1),$$

$$\partial M/\partial X=(M_2-M_1)/(X_2-X_1),$$

$$\partial N/\partial X=(N_2-N_1)/(X_2-X_1).$$

Similarly, variations of Y and Z yield the other difference quotients. When Z is varied we have to recalculate the functions $V_f(z)$ and $V_b(z)$ and the eigenvalue λ_p.

One arrives then at the linear system

$$\begin{bmatrix}X_1\\Y_1\\Z_1\end{bmatrix}=\begin{bmatrix}X\\Y\\Z\end{bmatrix}+\begin{bmatrix}\partial L/\partial X & \partial L/\partial Y & \partial L/\partial Z\\ \partial M/\partial X & \partial M/\partial Y & \partial M/\partial Z\\ \partial N/\partial X & \partial N/\partial Y & \partial N/\partial Z\end{bmatrix}\begin{bmatrix}dX\\dY\\dZ\end{bmatrix}.$$

The values obtained for X,Y,Z are closer to the solution and will be used as initial values in a repetition of the procedure. Three loops are sufficient to arrive at a relative precision of 10^{-5}. The solution obtained for the central frequency is now used as initial values in a similar calculation for a neighboring frequency, and so on. The calculation is terminated when the intensity reaches the value zero.

We have not yet calculated the optical length of the laser which would permit us to study the nonlinear displacements of the frequency (push-pull effect).

C. Numerical results

The numerical results we are going to describe in this paragraph correspond to a HeNe laser operating at 3.39μ. For the atoms we have taken a ratio of $\gamma_{ab}/kv_M=0.3$ where γ_{ab} is the inverse lifetime of optical coherence and kv_M is the half-width of the Doppler profile. These data fix the plasma dispersion function[18] which appears in the expressions for the coefficients α_0, β_1, and β_2. The geometry of the laser is given by $R=600$ mm and $d=400$ mm.

Our main objective is to illustrate two important theoretical results: First the variation of line shapes due to the inhomogeneous distribution of amplifying atoms, and second the variation of line shapes with the inhomogeneity of the field.

Experimentally, the first type of inhomogeneity can be varied by changing either the diameter of the tube or the intensity of the discharge current. We will give three series of curves (Figs. 5—7) all corresponding to the same data with the exception of the parameter u [cf. Eq. (36)]. An increase of u means an increase of the degree of inhomogeneity of active atoms.

Figure 5 corresponds to a value of $u=W_0^2/4$ which is consistent with a tube of 4-mm diameter and a parabolic distribution of amplifying atoms which vanishes at the boundary. We have drawn five curves, numbered 1 through 5 in each series, which correspond to five values of the indicated round-trip gain for the amplitude.

Figures 5(a)—5(c) describe, respectively, the intensity on the axis as it can be measured by a small area detector near the concave mirror, the variation of $W(d)^2$, and the variation of $R(d)$, i.e., the radius of curvature of the Gaussian beam at $z=d$. The medium fills the entire cavity. The diaphragm is placed on the concave mirror, its diameter is $2b=2.6$ mm, so that $b/W(d)=1.36$. Since the value of u is small, the saturation effect overpowers the effect due to inhomogeneity of the active population and the maximum of the intensity is found on the side of lower frequencies, as usual in the case of pure self-focusing or defocusing effects.[11] In Fig. 5(b), the variation of $W(d)^2$ shows a form of dispersion which agrees with previous calculations[11] and experiments.[8,12] In that figure, ${}^0W(d)^2$ denotes the value for the passive cavity. The variation of $R(d)$, which is the cause for the asymmetry of the gain, has its extremum on the side of low frequencies.

Figures 6 and 7 give the same type of results as Fig. 5, however, for parameter values $u=W_0^2/(0.9)^2$

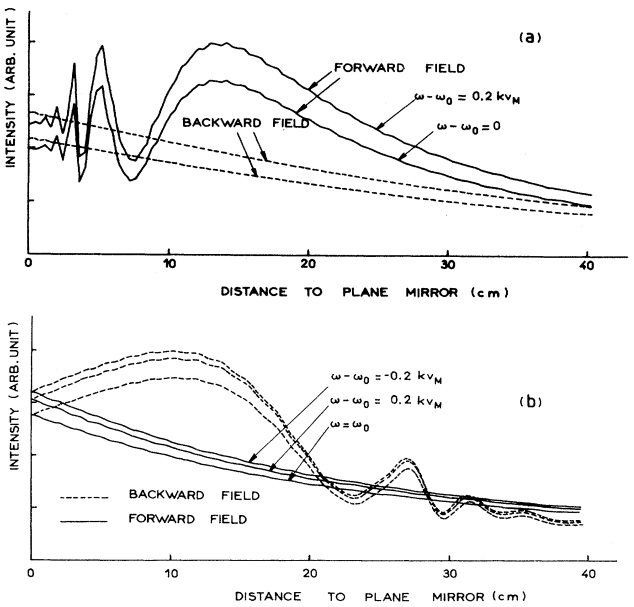

FIG. 8. Distribution of the diffracted field along the laser axis (a) when the diaphragm is on the plane mirror and (b) when it is on the concave mirror. Curves are drawn for various frequencies. (a): 100 Laguerre polynomials, $b/W_0=1.3$, gain 1.42, $u=W_0^2/1.4$, $\tilde{\rho}=1.5$. (b): 60 Laguerre polynomials, $b/W(d)=1.36$, gain 1.45, $u=W_0^2/0.81$, $\tilde{\rho}=1.5$.

(Fig. 6) and $u=W_0^2/(0.85)^2$ (Fig. 7). Figure 6(a) shows an evolution of the line shape: With increasing gain the curves become more and more symmetric. This is due to an increase of saturation inhomogeneity which overcomes the effect of the inhomogeneity in the distribution of amplifying atoms.

Figure 7(a) shows the line shapes in the case where the population inhomogeneity is large: The maximum of the intensity is now on the side of the higher frequencies.

The three figures 5, 6, and 7 show that the inhomogeneity of the population plays an important role in the formation of line shapes. This effect has been observed in experiments by Abraham and Kranz[22] using the 3.5-μm line of Xe. They found that a variation of the discharge current can give rise to a change in the asymmetry of the line. The theory presented in our work furnishes an explanation for this observation: In the case of weak currents, the population inhomogeneity is large and one finds the maximum of intensity on the high-frequency side. If the current is increased, the population inhomogeneity decreases and the intensity maximum shifts to the low-frequency side. One would expect that the same phenomenon should be observed also with the 3.39-μm line of Ne. First observational results[23] which we have obtained confirm this expectation. The situation is different for the line at 6328 Å since there, because of the much smaller diameter of the mode, one would need a very large population inhomogeneity to observe the effect.

We have made calculations identical to those whose results are described above, but for the case where the diaphragm is placed on the plane mirror. The results are qualitatively the same as before, apart from the fact that one now has a different distribution of the field in the cavity. Figures 8(a) and 8(b) which give the distributions of the on-axis intensity for different frequencies in the two cases, show that the variation of η^i is too small to introduce a noticeable dependence of the diffraction figure on the frequency and that the essential phenomenon is a translation of the intensity with frequency. We think that the variation of the figure of diffraction with frequency could be obtained if the term

$$G_p(\rho,\zeta)\exp[-i(\epsilon_{fp}-\tfrac{1}{2}\rho^2\eta_{fp})]\times 4ip(1-L_{p-1}/L_p)\eta_{fp}$$

which occurred in Eq. (49) and which we have neglected in the numerical calculation could be taken into account.

The curves of Figs. 4 and 8 show that two regions should be distinguished in a diaphragmed laser: One region on the side of the plane mirror where the intensity is increased, and the other region on the side of the concave mirror where the intensity is much weaker. The existence of these regions suggests calculations for the two cases where the amplifying medium, instead of filling the entire cavity, is placed in one or the other of them. We have adapted the program to these cases simply by setting $\alpha_0=\beta_1=\beta_2=0$ in the regions in which there is no amplification. We thus consider a situation where the amplifying tube has just half the length (200 mm) of the cavity. The diaphragm is placed on the side of the plane mirror. Figure 9 shows the results when the tube is placed in the region of high intensity on the side of the plane mirror. Figure 9(a) shows the intensity curves: The saturation is strong and the maximum of the intensity is on the side of the lower frequencies. Figure 10 shows the results for the case in which the tube is placed at the concave mirror: Due to the dominating effect of the population inhomogeneity, and to different boundary conditions, the line shapes show an asymmetry in the opposite sense. In both cases the same sets of parameters were used. We also remark that between the two regions there should be a position of the tube where one would obtain quasisymmetric line shapes, but where the asymmetry would be particularly sensitive to changes of the discharge current,

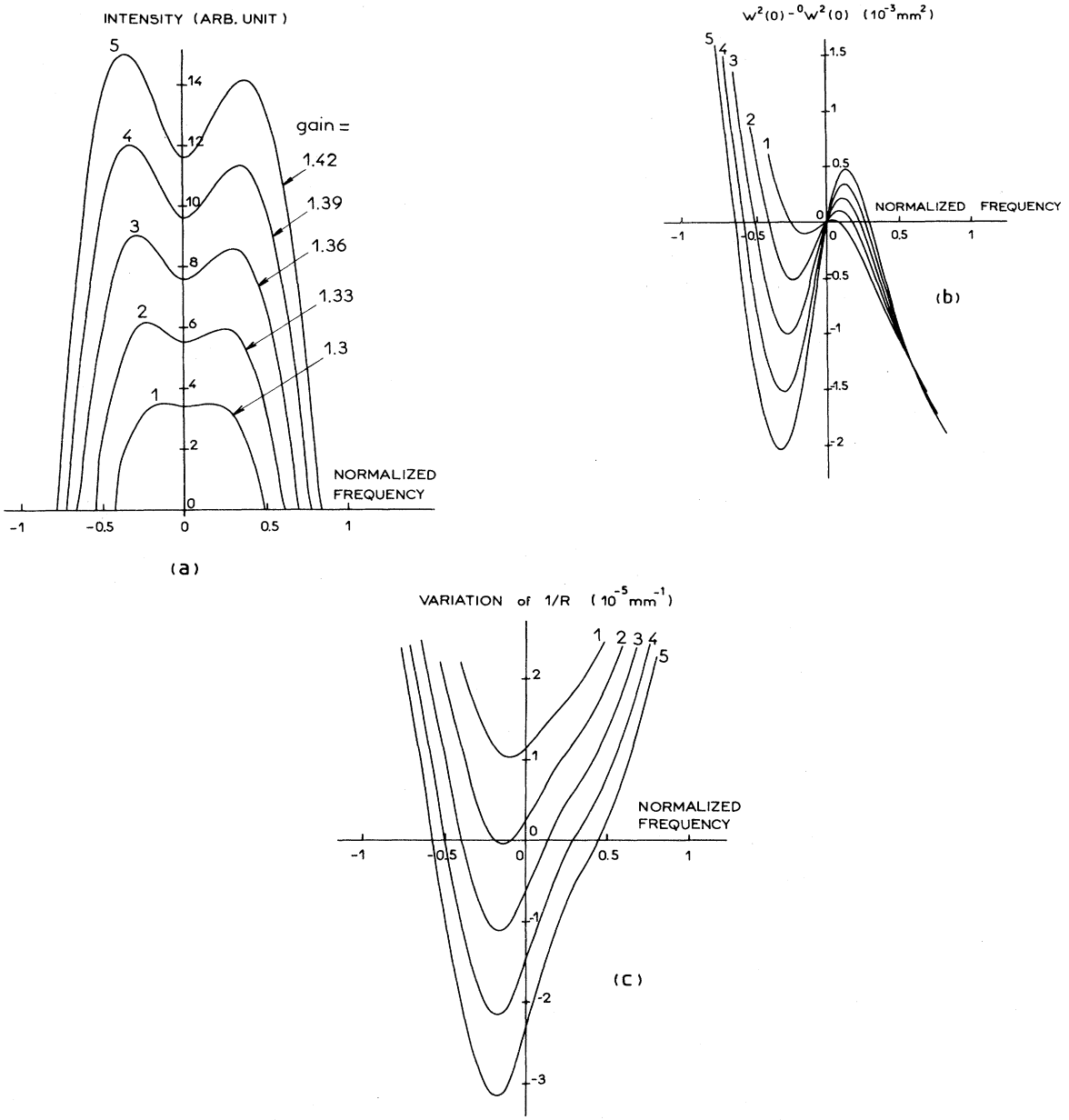

FIG. 9. Some characteristic features of the laser light vs reduced frequency as in Figs. 5—7, but with an amplifying medium filling only half the cavity on the side of the plane mirror. Dominant inhomogeneity which fixes the asymmetry is due to saturation. In contrast to the preceding, Figs. 5—7, the diaphragm is on the plane mirror and the quantities pictured were calculated at $z=0$. With the diaphragm on the concave mirror (not shown) we obtain the same results (even more pronounced). Parameters are $b/W_0=1.3$, $u=W_0^2/1.96$, $\tilde{\rho}=1.5$.

i.e., to the variation of the population inhomogeneity, or, more generally, to any cause which can vary either kind of inhomogeneity.

We have then illustrated the competition between the two lens effects which determine, sometimes in a critical manner, the asymmetry of the line: If the physical parameters of a particular laser favor inhomogeneity of saturation (this is the general case), one obtains a line shape having its maximum on the low-frequency side. If they favor inhomogeneity of population, the maximum is on the high-frequency side. These physical parameters are not only related to the geometry of the laser, but also to the transverse distribution of amplifying atoms which depends on the current, the pressure, the composition of the gas, and even on the nature of the boundary of the tube. We have not included in our calculation any longitudinal variation in the distribution of am-

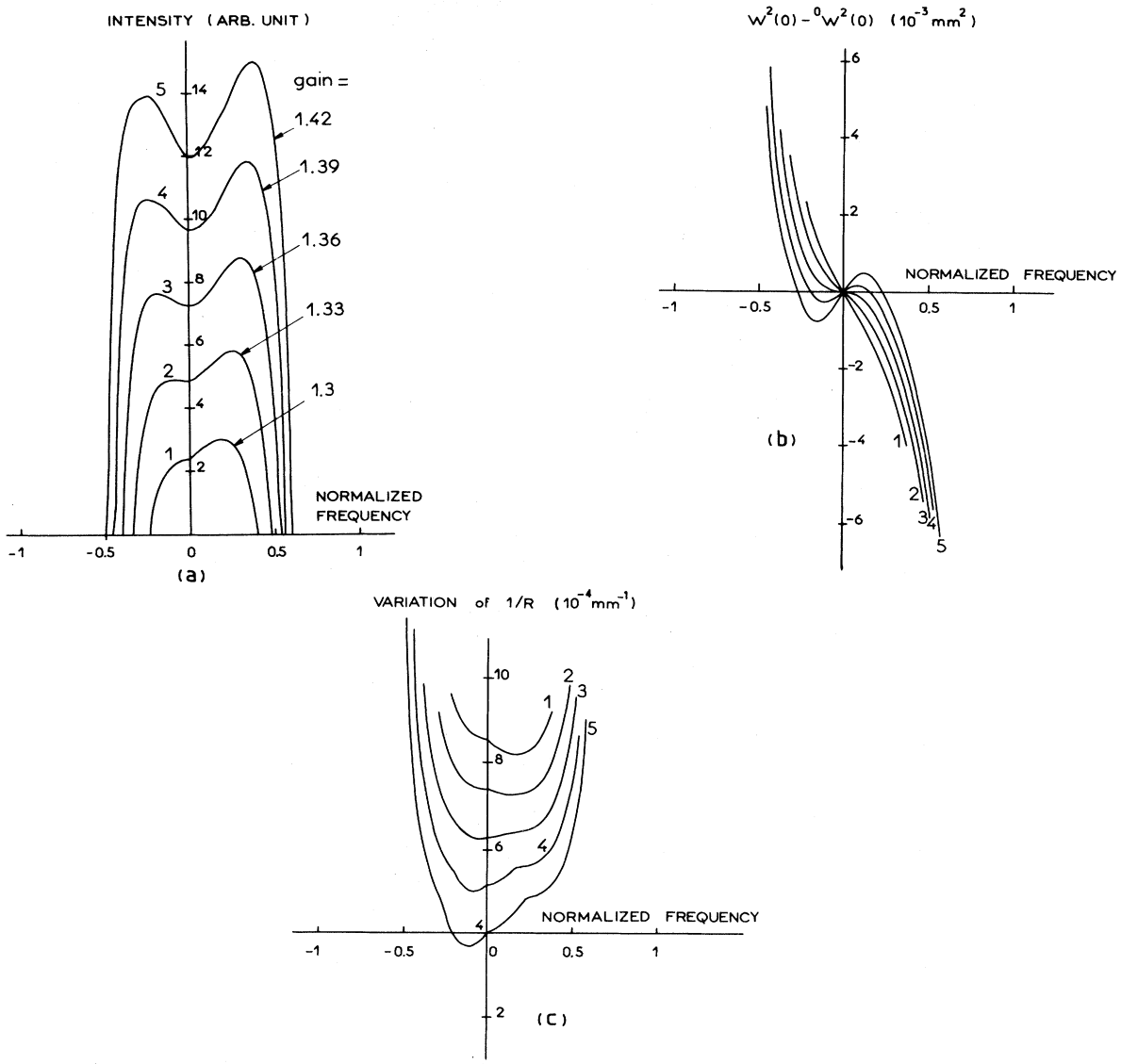

FIG. 10. Same as in Fig. 9, but with the amplifying medium filling half the tube on the side of the concave mirror. In this case, the saturation inhomogeneity is weak and the dominant process determining the asymmetry of the line is the population inhomogeneity. Figures 9 and 10 show that in the case where the two inhomogeneity effects balance each other one can get either asymmetry depending on the position of the amplifying tube inside the cavity. Same result, in even more pronounced form, is obtained when the diaphragm is on the concave mirror. Figures 9(b) and 10(b) as well as Figs. 9(c) and 10(c) show the same evolution as those previously illustrated in Figs. 5(b), 6(b), and (7b) and 5(c), 6(c), and 7(c).

plifying atoms, though this effect has been shown to exist at times.[16] Our present calculations are restricted to a single length of the cavity, but one can also predict line-shape variations for the cases where either the length of the amplifying tube, length of the cavity, or the position of the amplifying tube in the cavity are varied.

CONCLUSION

We have developed and investigated a new model of a gas laser which approximates reality better than previous ones: Physical characteristics of the laser (length of cavity, radius of curvature and reflectivity of mirrors, and position and size of diaphragm) are taken into account. We have set up the beam equation incorporating the inhomogeneity of the medium and have developed a method of solving it. We have further clarified the different roles played by the transverse inhomogeneity of the saturation and by the distribution of active atoms.

Also, we have introduced and calculated the resonant field distribution in a diaphragmed laser and thereby demonstrated the presence of a longitu-

dinal inhomogeneity of the saturation. Finally, we have calculated the line shapes corresponding to a variety of experimental conditions. On the basis of our results we can predict that line shapes change with the different types of inhomogeneities which exist in the amplifying medium and which themselves depend on macroscopic physical parameters of the laser such as the diameter and the form of the tube, position of the tube in the cavity, curvature and reflectance of the mirrors, distance of the mirrors, position and diameter of the diaphragm, discharge current, and pressure and composition of gases. When the beam diameter becomes comparable to a characteristic length describing the inhomogeneity of the population, the line shapes are very sensitive to the parameters mentioned before, as has been shown, for instance, in the case of the 3.39-μm line in Ne, or the 3.52-μm line in Xe. For lines in the visible range as, e.g., the 632.8-nm line of Ne, the diameter of the mode in much smaller and the asymmetry of the line is, in general, determined by the self-focusing and defocusing effects.

Our study explains some recently observed phenomena. Abraham and Kranz[22] discovered a change of asymmetry of the 3.52-μm line of Xe with a variation of the discharge current. We have made the same observation[23] on the 3.39-μm line of Ne.

This work thus demonstrates the important role played by macroscopic inhomogeneities in the explanation of line shapes.

ACKNOWLEDGMENT

We thank Professor N. B. Abraham for making his results available to us prior to publication.

---

*Present address: Institut für Theoretische Physik, Universität Göttingen, Bunsenstrasse 9, D-3400 Göttingen, Federal Republic of Germany.

[1]W. E. Lamb, Jr., Phys. Rev. 134, A1429 (1964).

[2]M. Sargent III, M. D. Scully, and W. E. Lamb, Jr., *Laser Physics* (Addison-Wesley, New York, 1974).

[3]R. H. Cordover and P. A. Bonczyk, Phys. Rev. 188, 696 (1969); A. Szöke and A. Javan, Phys. Rev. 145, 137 (1966); P. W. Smith, J. Appl. Phys. 37, 2089 (1966).

[4]B. L. Gyorffy, M. Borenstein, and W. E. Lamb, Jr., Phys. Rev. 169, 340 (1968); R. L. Fork and M. A. Pollack, Phys. Rev. 139, A1408 (1965).

[5]H. W. Kogelnik, Appl. Opt. 4, 1562 (1965); H. W. Kogelnik and T. Li, Appl. Opt. 5, 1550 (1966).

[6]H. Maeda and K. Shimoda, J. Appl. Phys. 46, 1235 (1975).

[7]B. K. Garside, IEEE J. Quantum Electron. QE-4, 940 (1968).

[8]A. Le Floch, R. Le Naour, J. M. Le Normand, and J. P. Taché, Phys. Rev. Lett. 45, 544 (1980).

[9]L. W. Casperson and A. Yariv, Appl. Opt. 11, 462 (1972).

[10]C. J. Borde, G. Camy, and B. Decomps, Phys. Rev. A 20, 254 (1979).

[11]G. Stephan and H. Taleb, J. Phys. (Paris) 42, 1623 (1981).

[12]G. Stephan, H. Taleb, C. Pesty, and F. Legros, J. Phys. (Paris) 43, 255 (1982).

[13]M. Lax, W. H. Louisell, and W. B. McKnight, Phys. Rev. A 11, 1365 (1975).

[14]M. Nazarathy, A. Hardy, and J. Shamir, J. Opt. Soc. Am. 72, 1409 (1982) and references therein. See also L. W. Casperson, Appl. Opt. 12, 2434 (1973).

[15]G. Arfken, *Mathematical Methods for Physicists,* 2nd ed. (Academic, New York, 1973), p. 616.

[16]I. P. Mazanko, M. I. Molchanov, N. D. D. Ogurok, and M. V. Sviridov, Opt. Spektrosk. 30, 927 (1971) [Opt. Spectrosc. (U.S.S.R.) 30, 495 (1971)].

[17]P. A. Wolff, N. B. Abraham, and S. R. Smith, IEEE J. Quantum Electron. QE-13, 400 (1977).

[18]G. Stephan, R. Le Naour, and A. Le Floch, Phys. Rev. A 17, 733 (1978).

[19]C. J. Borde, in *Laser Spectroscopy III,* edited by J. C. Hall and J. L. Carlsten (Springer, Berlin, 1977), p. 121.

[20]H. J. Caulfield, D. Dvore, J. W. Goodman, and W. Rhodes, Appl. Opt. 20, 2263 (1981).

[21]G. Otis, J.-L. Lachambre, and P. Lavigne, Appl. Opt. 18, 875 (1979).

[22]N. B. Abraham (private communication).

[23]G. Stephan (unpublished).